Age and diet modulate the insulin-sensitizing effects of exercise

Vieira-Lara, Marcel A; Reijne, Aaffien C; Koshian, Serj; Ciapaite, Jolita; Abegaz, Fentaw; Talarovicova, Alzbeta; van Dijk, Theo H; Versloot, Christian J; Bandsma, Robert H J; Wolters, Justina C

Published in:
Diabetes

DOI:
10.2337/db22-0746

Publication date:
2023

Age and Diet Modulate the Insulin-Sensitizing Effects of Exercise: A Tracer-Based Oral Glucose Tolerance Test

Marcel A. Vieira-Lara,[1] Aaffien C. Reijne,[1,2] Serj Koshian,[1] Jolita Ciapaite,[1] Fentaw Abegaz,[1] Alzbeta Talarovicova,[1,2] Theo H. van Dijk,[3] Christian J. Versloot,[1,4] Robert H.J. Bandsma,[1,4] Justina C. Wolters,[1] Albert K. Groen,[5] Dirk-Jan Reijngoud,[1] Gertjan van Dijk,[2] and Barbara M. Bakker[1]

Diabetes 2023;72:872–883 | https://doi.org/10.2337/db22-0746

Diet modulates the development of insulin resistance during aging. This includes tissue-specific alterations in insulin signaling and mitochondrial function, which ultimately affect glucose homeostasis. Exercise stimulates glucose clearance and mitochondrial lipid oxidation and also enhances insulin sensitivity (IS). It is not well known how exercise interacts with age and diet in the development of insulin resistance. To investigate this, oral glucose tolerance tests with tracers were conducted in mice ranging from 4 to 21 months of age, fed a low-fat diet (LFD) or high-fat diet (HFD) with or without life-long voluntary access to a running wheel (RW). We developed a computational model to derive glucose fluxes, which were commensurate with independent values from steady-state tracer infusions. Values for an IS index derived for peripheral tissues (IS-P) and one for the liver (IS-L) were steeply decreased by aging and an HFD. This preceded the age-dependent decline in the mitochondrial capacity to oxidize lipids. In young animals fed an LFD, RW access enhanced the IS-P concomitantly with the muscle β-oxidation capacity. Surprisingly, RW access completely prevented the age-dependent IS-L decrease; however this only occurred in animals fed an LFD. Therefore, this study indicates that endurance exercise can improve the age-dependent decline in organ-specific IS if paired with a healthy diet.

ARTICLE HIGHLIGHTS

- Exercise is a known strategy to improve insulin sensitivity (IS), whereas aging and a lipid-rich diet decrease IS.
- Using a tracer-based oral glucose tolerance test, we investigated how exercise, age, and diet interact in the development of tissue-specific insulin resistance.
- Exercise (voluntary access to a running wheel) mainly improved IS in animals fed a low-fat diet. In these animals, exercise improved peripheral IS only at young age but fully prevented the age-dependent decline of hepatic IS.
- The prevention of age-dependent decline in IS by exercise is tissue-specific and blunted by a lipid-rich diet.

Aging, diet, and exercise have a profound effect on insulin sensitivity (IS) and glucose homeostasis (1–3). Consequently, they affect the emergence of insulin resistance, a pathophysiological process that precedes the development of type 2 diabetes. Insulin resistance is characterized by decreased insulin-stimulated glucose uptake and decreased insulin-dependent suppression of the endogenous glucose production (EGP) (2). In the postprandial state, together with the central nervous system, the skeletal muscle represents

[1]Laboratory of Pediatrics, Center for Liver, Digestive, and Metabolic Diseases, University Medical Center Groningen, University of Groningen, Groningen, the Netherlands
[2]Groningen Institute for Evolutionary Life Sciences, Department of Behavioral Neuroscience, University of Groningen, Groningen, the Netherlands
[3]Department of Laboratory Medicine, University Medical Center Groningen, University of Groningen, Groningen, the Netherlands
[4]Translational Medicine, Peter Gilgan Centre for Research and Learning, The Hospital for Sick Children, Toronto, Ontario, Canada
[5]Department of Vascular Medicine, Amsterdam University Medical Centers, Amsterdam, the Netherlands

Corresponding authors: Gertjan van Dijk, gertjan.van.dijk@rug.nl, and Barbara M. Bakker, b.m.bakker01@umcg.nl

Received 1 September 2022 and accepted 19 April 2023

This article contains supplementary material online at https://doi.org/10.2337/figshare.22665826.

M.A.V.-L. and A.C.R. contributed equally to this work. G.v.D. and B.M.B. contributed equally to this work.

one of the major sites for glucose clearance, whereas the main site of EGP is the liver (4–6). Insulin resistance in the skeletal muscle and the liver can be induced by the accumulation of lipids, which involves the inhibition of the insulin signaling cascade by complex lipids (2). This lipid-induced insulin resistance can be elicited in mice fed a high-fat diet (HFD) (7). It is questionable, however, whether insulin resistance development is caused by an overload of substrate (8), by a loss of mitochondrial flexibility and/or function (9,10), or a combination of both.

Aging exacerbates the susceptibility to lipid-induced insulin resistance (11,12), which, among other factors, involves changes in lipid handling, both in the skeletal muscle (11,13) and the liver (14). The main route for lipid oxidation is the mitochondrial fatty-acid β-oxidation, with its flux being mostly controlled at the level of carnitine palmitoyltransferase 1 (CPT1) (13,15). We previously reported that an inability of old animals to upregulate muscle CPT1B (the muscle isoform) in response to an HFDfunctioned as a basis for insulin resistance development (13). Aging is also a risk factor for insulin resistance on its own (1), and its association with sarcopenia (loss of muscle mass) (16) may further exacerbate insulin resistance (17).

In humans, both resistance (strength) and endurance (aerobic) exercise have been associated with improved IS (18,19). Whereas resistance training rescues age-related muscle loss (20), endurance training is generally more effective in improving mitochondrial function in aging (16,21,22). The high mitochondrial capacity of endurance-trained athletes protects against lipid-induced insulin resistance (23,24). With aging, however, the link between mitochondrial capacity and IS as a result of exercise may disappear: It was found that aerobic exercise improved oxidative capacity irrespective of age, whereas it only improved IS in young people (24). Access to a running wheel (RW) is a widely used protocol to study the effects of endurance exercise in mice (25). In line with the above, in mice ranging from 6 to 24 months old, RW access increased mitochondrial content and oxidative capacity in the quadriceps, irrespective of whether a low-fat diet (LFD) or HFD was given. This was dissociated from the age-related decline in muscle weight (26). Finally, exercise affects IS and glucose handling in the muscle and the liver (27,28). After long-term endurance training, the ability of the liver to take up glucose increases and so does its sensitivity to insulin (27).

Although the effects of endurance exercise have been studied at different ages and on different diets, it has not been systematically addressed how these three factors interact in the development of muscle and liver insulin resistance. Moreover, a tissue-specific analysis of insulin resistance and glucose handling is crucial to dissect the role of mitochondrial function in insulin resistance. For this purpose, indices that distinguish muscle (peripheral) and liver IS are necessary. The frequently used HOMA-IR index is a measure of whole-body IS based on fasting glucose levels. An oral glucose tolerance test (OGTT) is used to derive the Muscle Insulin Sensitivity Index (MISI; focused on peripheral IS) or a Matsuda index (whole-body IS) during a glucose load (5,29,30). Including a stable-isotope-labeled glucose tracer to either oral or intravenous (IV) glucose tolerance tests enables one to dissect the contribution of the EGP from that of the glucose elimination by the muscle and other peripheral tissues and enables one to quantify IS in a tissue-specific manner (31–34). In the present study, we combine this advantage of a tracer with the OGTT.

Here, we investigate the combined effects of age, diet, and voluntary wheel running on glucose homeostasis and tissue specific IS in a cohort of aging mice about which we reported previously (26,35). To this end, we applied an existing OGTT protocol with [6,6-$^2H_2$]-glucose in mice (36) and adapted a computational model from earlier work in humans (37).

RESEARCH DESIGN AND METHODS

Mouse Experiments and Ethics Approval

Mouse experiments were performed as previously described (26,35). Briefly, male C57BL/6JOlaHsd mice (Jackson Laboratory, Bar Harbor, ME) were maintained at 22°C on a 12-h light/12-h dark cycle and ad libitum access to an LFD (6% calories from fat, 1% w/w sugar; AMII 2141, HopeFarms BV, Woerden, the Netherlands). On postnatal day 28, mice were placed in individual cages (Makrolon type II; Bayer) and given either the same LFD or an HFD high in sucrose during their entire lifetime (45% calories from fat, 20% w/w sucrose; 4031.09, HopeFarms BV). A total of 128 mice were randomly subdivided into voluntary RW groups or sedentary controls (Ctrl). At the age of 4, 9, 15, or 21 months (used throughout the text to define the age groups), animals underwent an OGTT with a tracer (Fig. 1*A*). The same animals underwent steady-state IV infusion (SS-IV) experiments (38) at the age of 6, 12, 18, or 24 months, respectively, after which animals were terminated and the quadriceps and liver were collected, as previously described (26).

To determine the bioavailability of the tracer, independent experiments were conducted in 3-week-old male C57BL/6J mice (Jackson Laboratory), fed an LFD (Teklab Custom Diet TD.10098; Envigo Teklad Diets, Madison, WI) for 2 weeks prior to tracer measurements. Animal experiments were approved by the Dutch Central Authority for Scientific Procedures on Animals and by the University of Groningen Ethical Committee for Animal Experiments.

OGTT With Glucose Tracer

On the day of the experiment, food was removed in the morning at 7:00 (winter) or 8:00 (summertime). The OGTT was conducted after a fasting period of 6 h (i.e., at 13:00 or 14:00). Body weight was measured before the start of the experiment. Access to an RW was maintained during the OGTT time frame. In the RW groups, the last bout of intense exercise occurred 6–7 h before the ingestion of the glucose bolus, according to data on average RW revolutions at different ages (Supplementary Fig. 1). At time point zero, a glucose bolus of 1 $g \cdot kg^{-1}$ ($5.5 \cdot 10^3$ $\mu mol \cdot kg^{-1}$) was administered orally. It consisted of 0.7 $g \cdot kg^{-1}$ ($3.9 \cdot 10^3$ $\mu mol \cdot kg^{-1}$) unlabeled

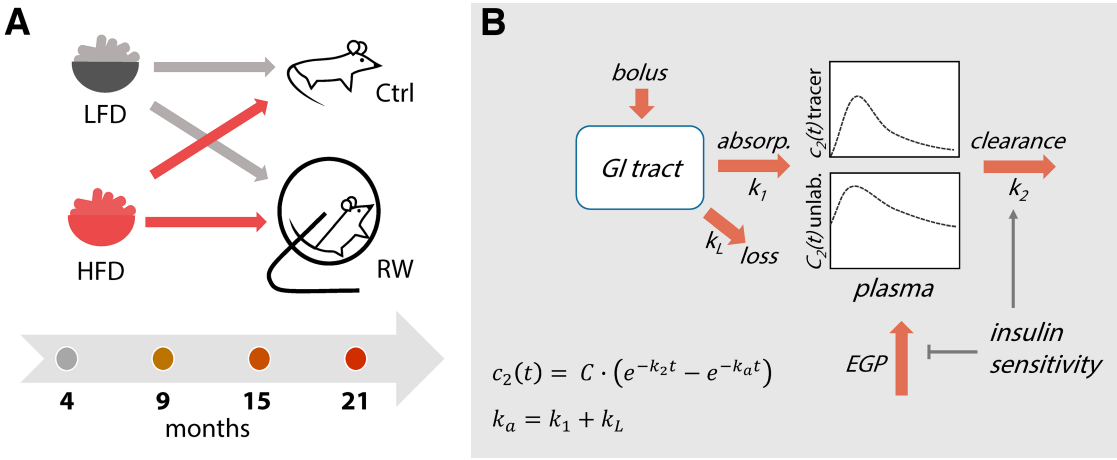

Figure 1—Schematic representation of experimental design (*A*) and compartment model for data analysis (*B*). GI, gastrointestinal; absorp., absorption flux into the plasma compartment, represented by the rate constant k_1; loss, loss flux from the GI compartment, represented by the rate constant k_L. Both tracer and unlabeled glucose in the plasma compartment can be cleared from the circulation, represented by the rate constant k_2. EGP by the liver feeds into the unlabeled glucose pool in the plasma. Insulin enhances the clearance of both tracer and glucose and inhibits the EGP. The apparent absorption constant k_a obtained from the tracer curves equals $k_1 + k_L$ (See *Research Design and Methods* for details).

glucose and 0.3 g · kg^{-1} (1.6 · 10^3 μmol · kg^{-1}) [6,6-^{2}H$_2$]-glucose (a tracer). Total blood glucose (Lifescan Euroflash; Lifescan Benelux, Beerse, Belgium) was measured from the tail vein, from which blood spots were also collected. Insulin was measured according to manufacturer instructions (Ultrasensitive Mouse Insulin kit; Mercodia, Uppsala, Sweden). The fractional contribution of the administered tracer in blood glucose (described below) was measured in air-dried blood spots. Glucose and tracer enrichment were measured at 0, 15, 30, 45, 60, 75, 90, 105, and 120 min and insulin was measured at 0, 30, and 60 min.

Bioavailability

Five-week-old animals from an independent cohort were fasted for 4 h and received an IV bolus of [6,6-^{2}H$_2$]-glucose (1.0 · 10^3 μmol · kg^{-1}) injected retro-orbitally. This was directly followed by an oral bolus containing glucose (2.0 · 10^3 μmol · kg^{-1}) and a tracer, [U-^{13}C]-glucose (70 μmol · kg^{-1}). Blood spots were collected at 0, 10, 20, 30, 40, 50, 60, and 90 min, and glucose was measured as described above. Air-dried blood spots were used for posterior analysis of fractional abundance.

Gas Chromatography Coupled to Mass Spectrometry and Isotope Correction

Fractional distributions of [6,6-^{2}H$_2$]-glucose and [U-^{13}C]-glucose in blood spots were measured according to van Dijk et al. (38). Glucose was converted into its pentaacetate derivative by adding a pyridine–acetic anhydride mixture. All samples were analyzed by gas chromatography coupled to mass spectrometry (Agilent 9575C inert MSD; Agilent Technologies, Amstelveen, the Netherlands). Derivatives were separated on an AT-1701 30 m × 0.25 mm ID (0.25-μm film thickness) capillary column (Alltech, Breda, the Netherlands).

The monitored isotopologue distribution (*m/z* 408–414) was corrected for the natural abundance of isotopes based on the approach using the measured isotopologue distribution in the baseline samples, as described in the Supplementary Material. Tracer concentrations were obtained by multiplying the corrected fractional abundance of the *m/z* 410 isotopologue for [6,6-^{2}H$_2$]-glucose and *m/z* 414 for [U-^{13}C]-glucose by the corresponding total glucose concentration. Unlabeled glucose concentrations were obtained by subtracting tracer concentrations from the total measured glucose concentrations.

Modeling Strategy

To derive the kinetic constants from the tracer data, we considered two compartments: the gastrointestinal tract compartment (compartment 1) and the blood plasma (compartment 2) (Fig. 1*B*). The pool sizes (q) and concentrations (c) of the tracer in these compartments are denoted by q_1, q_2, c_1, and c_2 and those of unlabeled glucose analogously by Q_1, Q_2, C_1, and C_2, with the subscript specifying the compartment. Pool sizes Q and q were expressed in μmol · kg^{-1} (referring to kg of body weight), whereas concentrations C and c were expressed in mmol/L. Inspired by the experimental setup, the model was confined to the pool size of the glucose that was administered in the stomach by oral gavage and dosed in μmol · kg^{-1} (Q_1, q_1) and by the plasma concentrations (C_2, c_2) that were measured in mmol/L. All modeling details can be found in the Supplementary Appendix.

CPT1 Quantification and Oxidative Capacity

Mitochondria were isolated from quadriceps and liver tissue, as previously described (26,39). CPT1A and CPT1B protein levels were quantified by targeted proteomics in isolated

mitochondrial suspensions (40). Oxygen consumption rates were measured in MiR05 buffer (41) in a two-channel, high-resolution Oroboros oxygraph-2k (Innsbruck, Austria). Palmitoyl-CoA (25 μmol/L), L-carnitine (2 mmol/L) and malate (2 mmol/L) were used as substrates. Maximal ADP-stimulated respiration was measured after the addition of 1.5 U/mL hexokinase, 12.5 mmol/L glucose, and 1 mmol/L ATP. Protein content was measured with the Pierce BCA Protein Assay Kit (Thermo Fisher; catalog 23225). The ratio of cytosolic to mitochondrial protein was determined as previously described (26) and used to express CPT1 content and oxidative capacity per total tissue protein.

Software and Analysis

Correction for natural abundance was performed in Excel 2019. All other calculations and simulations were conducted in Python (version 3.7) using Jupyter Notebook (version 5.7.4). Parameters from the tracer kinetics and curves for the unlabeled glucose were estimated with the *minimize* function from the *lmfit* Python package (Levenberg-Marquardt method, nonlinear least squares). Data visualization and statistical analysis were conducted either in Python (*matplotlib, scipy*) or GraphPad Prism (version 9.0; GraphPad Software, San Diego, CA). Statistical analyses comparing the effects of age, diet, and exercise, as well as their interaction, were conducted by three-way ANOVA.

Data and Resource Availability

All data generated or analyzed during this study are included in the published article and its online supplementary files. The resources generated during this study can be found at github.com/mvieiralara/OGTT_modelling.

RESULTS

HFD Reduces Glucose Elimination in an Age-Dependent Manner

Mice fed either an LFD or HFD were divided into a sedentary group (Ctrl) and a group with voluntary access to an RW. Physiological characteristics of these mice have been previously described (35). To study glucose kinetics and IS, a tracer OGTT was conducted in mice that were 4, 9, 15, or 21 months old (Fig. 1*A*). A computational model consisting of glucose absorption, loss, clearance, and EGP was built (Fig. 1*B* and Supplementary Material). The tracer time-course data were fitted to the equation in Fig. 1*B* (Fig. 2 and Supplementary Material).

The apparent rate constant of absorbance k_a (Fig. 1*B*) was higher in the HFD than in the LFD groups ($P_{\text{diet}} < 0.01$; Fig. 3*A*) and decreased with advanced age ($P_{\text{age}} < 0.001$; Fig. 3*A*). The apparent rate constant k_2 represents the fractional clearance rate of glucose from the plasma compartment ("glucose effectiveness"). The HFD decreased k_2 (vs. LFD; $P_{\text{diet}} < 0.001$), whereas k_2 responded differently to aging in each diet group ($P_{\text{age} \times \text{diet}} < 0.001$), with no effect of RW access. In an independent tracer experiment in which IV and oral administration of the tracer were compared, the bioavailability F was determined to be 0.8 (Fig. 3*C–F*), implying that 80% of the tracer is absorbed and 20% is lost from our observation. Thus, $k_1 = 0.8 \cdot k_a$ and $k_L = 0.2 \cdot k_a$ (compare with Fig. 1*B*). An 80% bioavailability is in agreement with previous studies in humans and dogs (42,43). The apparent volume of distribution (see *Vol*, Eq. 14 in Supplementary Material) was lower in the HFD group than in the LFD group ($P_{\text{diet}} < 0.001$) and responded in a diet-dependent manner to RW access ($P_{\text{diet} \times \text{RW}} < 0.01$) and age ($P_{\text{diet} \times \text{age}} < 0.05$) (Fig. 3*G*). In summary, all kinetic constants in the model could be obtained from the tracer OGTT if the bioavailability is independently determined. Moreover, the rate constant of glucose clearance was reduced by the HFD in an age-dependent manner.

The HFD treatment reduced the basal glucose disappearance rate (R_d) ($P_{\text{diet}} < 0.05$), whereas R_d was affected by age in a diet-dependent manner ($P_{\text{age} \times \text{diet}} < 0.001$) (Fig. 3*H*). Subsequently, these outcomes were compared with those of classical SS-IV experiments (38), which allow for a model-independent measurement of basal glucose fluxes. In the 4-month-old group, basal R_d^{SS-IV} values (Eq. 26 in Supplementary Material) were in the same range as those obtained from the tracer OGTT (Fig. 3*I*). Although this was true for all ages, the biological trends were not the same (Supplementary Fig. 2). This reflects the nature of the experiment: in the OGTT experiment, the k_2 was estimated over the entire time course, during which the glucose bolus stimulated the release of hormones such as insulin. In the steady-state experiment, only tracer was infused, which should have barely affected hormone production.

Advanced Age Leads to Decreased EGP

The time courses of unlabeled glucose (Fig. 4) depend on the same kinetic parameters as that of the tracer andthe EGP (Fig. 1*B*). The variation within the groups was larger for unlabeled than for labeled glucose (compare with Figs. 2 and 4), indicating more variation in the EGP component, which may reflect stress due to animal handling (44). Individual curves that did not show the typical absorption followed by a clearance phase occurred in all experimental groups and were excluded (Supplementary Fig. 3). Fasting glucose values (Supplementary Fig. 4) were elevated in the HFD group ($P_{\text{diet}} < 0.01$) and reduced by advanced aging ($P_{\text{age}} < 0.05$), which, in turn, was modulated by the RW ($P_{\text{RW} \times \text{age}} < 0.05$).

After administration of the glucose bolus, the EGP decreased initially in most groups, reaching a minimum between 5 and 20 min, before reaching a new stationary level (Fig. 5*A*). The initial decline can be attributed to the inhibitory effect of increased plasma insulin and glucose (45). The steady-state EGP was calculated as the average of the last 30 min (Fig. 5*B*), and the overall average EGP was calculated over the entire period from 5 to 120 min (Fig. 5*C*). Higher age decreased both steady-state and average EGP ($P_{\text{age}} < 0.01$) (Fig. 5*B* and *C*), which is in line with

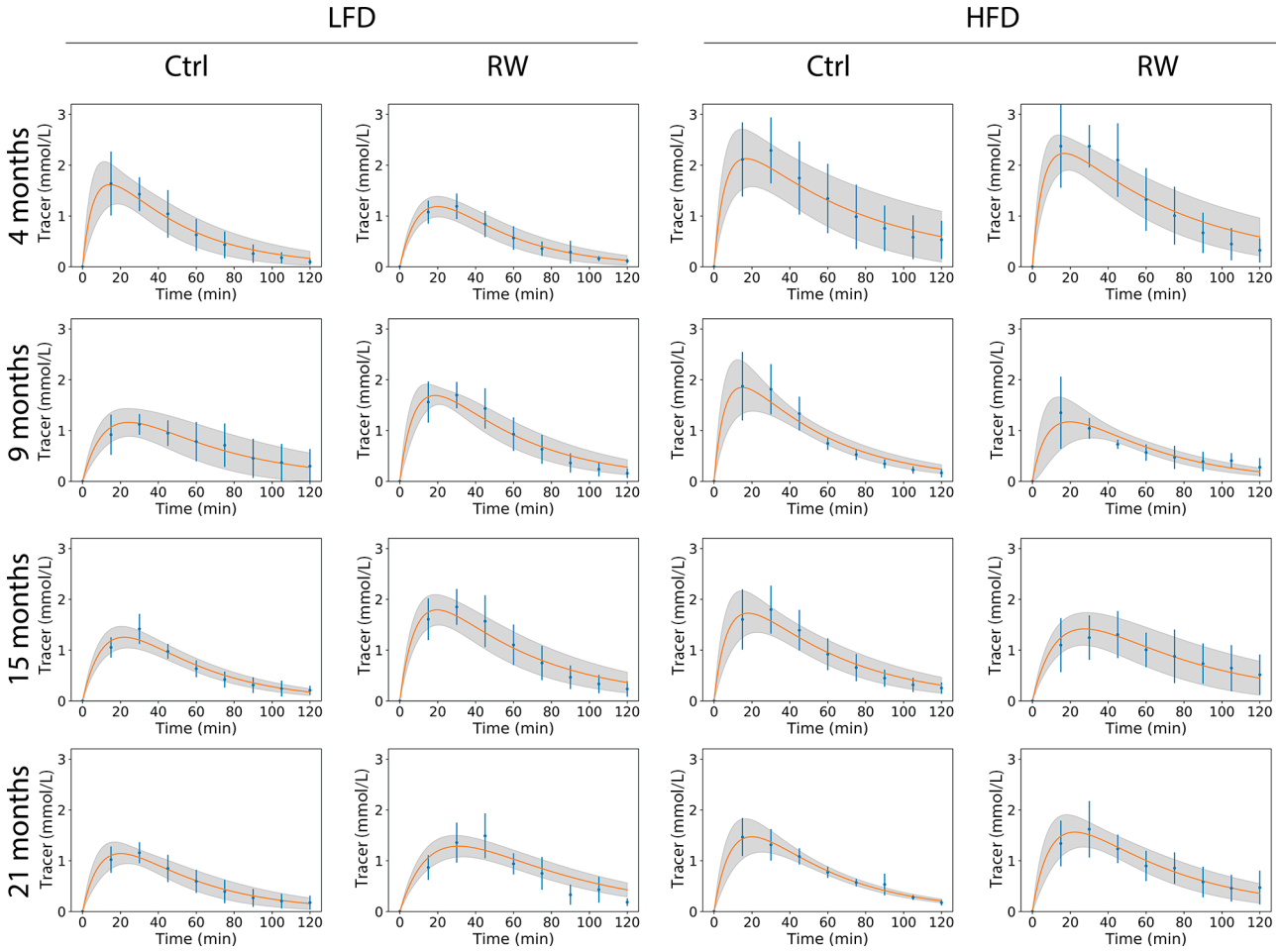

Figure 2—Curve fits for time courses of the [6,6-$^2H_2$]-glucose tracer during OGTT. Each column represents a different diet and activity group, whereas each row represents a different age. Mean ± SD for each time point are shown in blue. The average curve fit from all animals per experimental group (c_2 in the model) is shown in orange, with the SD of the fitted curves represented by the shaded area. n = 6–8 per group.

the usually lower glucose levels in older animals (Fig. 4). The RW generally decreased the steady-state and average EGP (vs. Ctrl, $P_{RW} < 0.05$), mostly in the LFD group ($P_{RW \times diet} < 0.05$). The calculation of EGP in μmol · kg^{-1} · min^{-1} (Fig. 5) depends on the assumption of constant bioavailability. When EGP is expressed in mmol/L · min^{-1} (denoted EGP*), it was independent of the bioavailability (Supplementary Material) and followed the same trend (Supplementary Fig. 5*A*) as in Fig. 5*A*. Similar patterns were also observed for steady-state and average EGP* (Supplementary Fig. 5*B* and *C*). This highlights that the differences between groups are independent of the assumption of constant bioavailability.

The steady-state EGP derived from the tracer OGTT (EGP^{OGTT}) was compared with independent SS-IV experiments conducted in the same cohort of animals. This yielded a model-independent basal EGP ($EGP^{SS\text{-}IV}$). EGP^{OGTT} and $EGP^{SS\text{-}IV}$ were similar to each other in 4-month-old animals (Fig. 5*D*). Although the same trend was observed in all age groups, the tracer OGTT usually yielded higher EGP values than the steady-state experiment (Fig. 5*D* and Supplementary Fig. 5D).

RW Access Mostly Affects Liver, Not Muscle, Insulin Sensitivity

Both age and an HFD strongly increased the insulin levels during the OGTT (for age and diet each, $P < 0.001$), in line with previous results (13,35), whereas RW access decreased insulin levels by ∼20% ($P_{RW} < 0.01$) (Fig. 6*A*). HOMA-IR, a classic surrogate index for whole-body insulin resistance, followed a pattern similar to that of average insulin levels (Fig. 6*B*). Age and an HFD (for age and diet each, $P < 0.001$) increased HOMA-IR, whereas the RW access reduced it ($P_{RW} < 0.05$). The effect of RW access was particularly pronounced in the LFD group.

Despite its wide application, the HOMA-IR does not capture organ-specific insulin resistance (5,46). We defined an IS index for peripheral tissues (IS-P) as the fractional clearance (k_2; min^{-1}) divided by the insulin concentration (mU · L^{-1}) (Eq. 29 in Supplementary Material; Fig. 6). In the LFD groups, the IS-P decreased strongly between 4 and 9 months in sedentary and RW groups. In the HFD groups, the IS-P was already low when mice were young (4 months) and did

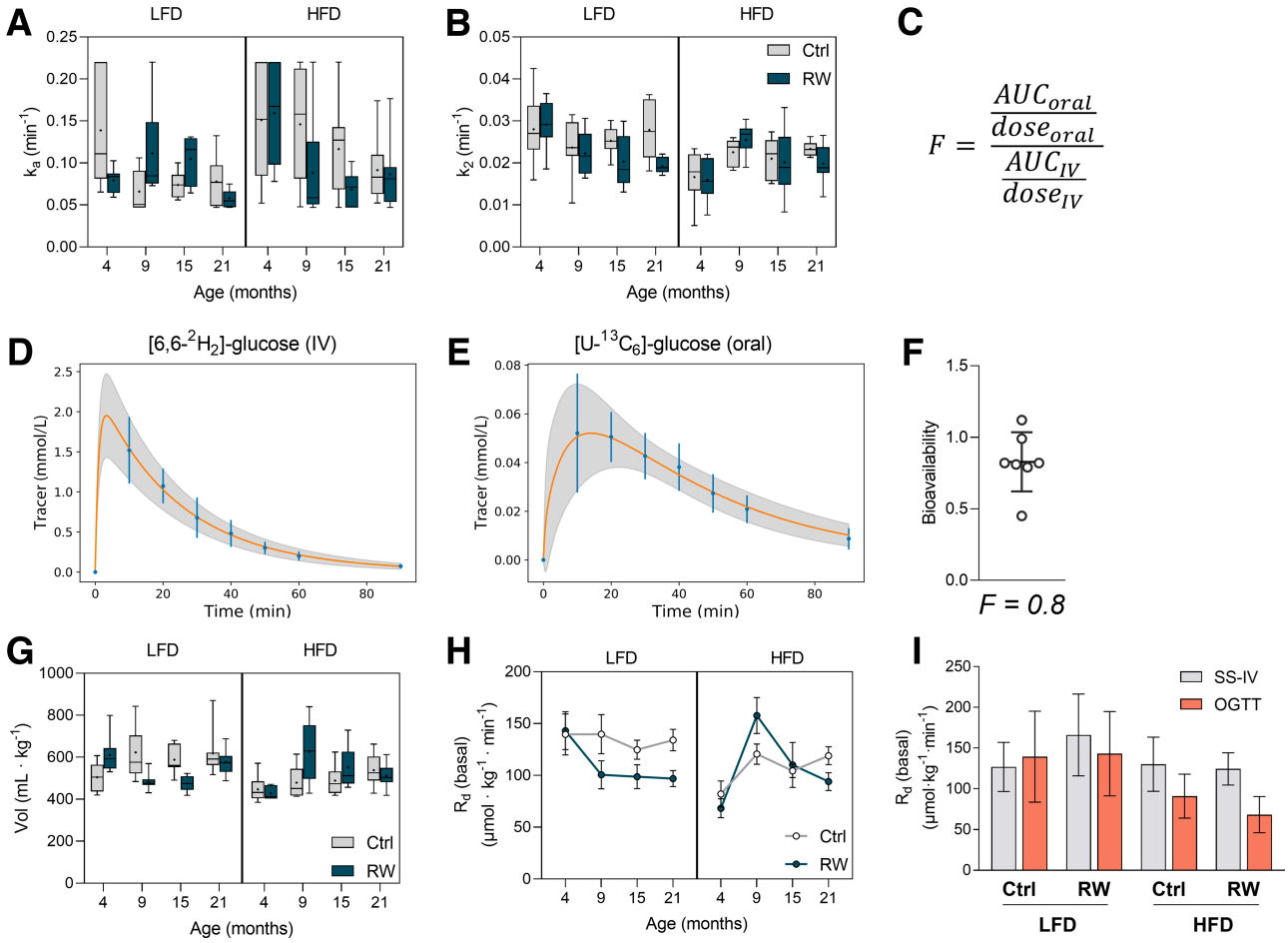

Figure 3—The HFD reduced both the rate constant and the rate of glucose elimination. Kinetic constants k_a (*A*) and k_2 (*B*) calculated from curve fits. Equation for calculating the bioavailability *F* based on IV and oral experiments, in which the areas under the curve (AUC) are corrected for the dose and then divided (*C*). To calculate *F*, curves were fitted to tracer time courses after either IV (*D*) or oral administration (*E*) of glucose to 5-week-old mice. Data points are shown in blue as mean ± SD (n = 8), and the average curve fit from all animals are in orange; the SD of the fitted curve is represented by the shaded area. Calculated bioavailability *F* (*F*). Apparent volume of distribution (*Vol*) assuming a constant *F* for all groups (*G*). Basal rate of disappearance of glucose (R_d) calculated from the OGTT data (mean ± SEM) (*H*). Comparison between R_d calculated from the tracer OGTT in 4-month-old animals and SS-IV experiments conducted in the same animals at 6 months. Data are shown as mean ± SD; n = 6–8 (*I*).

not decline further during aging (Fig. 6*C*). Together, age, diet, and their interaction explained more than 50% of the variation in the data set (for age, diet, and age × diet each, $P < 0.001$). RW access significantly increased the IS-P ($P_{RW} < 0.05$), particularly in the 4-month-old LFD group (~50% increase vs. Ctrl) (Fig. 6*C*). RW access alone, however, explained <2% of the variation in the data. The interaction terms RW × diet and RW × age had *P* values of 0.06 and 0.07, respectively, which point to a trend of differential effects of RW access in older HFD groups.

Insulin also regulates the EGP, although this regulation is more complex to analyze (47). We adapted a hepatic IS index that was originally based on fasting EGP and insulin levels (29). Instead, we used the time-averaged EGP and insulin levels to apply the IS index for the liver (IS-L) to the postprandial state mimicked by the tracer OGTT (Eq. 30 in Supplementary Material and Fig. 6). Similar to the IS-P, the IS-L was strongly reduced by aging, and again, to a smaller extent, in the HFD group in which the IS-L was already low from 4 months of age (Fig. 6*D*). Surprisingly, in the LFD group, RW access strongly enhanced the IS-L, more than it affected the IS-P, thus delaying the age-related loss of the hepatic IS (Fig. 6*D*). Using the EGP* (Supplementary Fig. 5*C*) yielded the same pattern for the IS-L (Supplementary Fig. 6*A*), which reiterates that the effects of age, diet, and RW access do not depend on the assumption of constant tracer bioavailability.

Both IS-P and IS-L correlated with the HOMA-IR (Supplementary Fig. 6*B* and *C*). The differences between IS-P and IS-L curves warrant a strict dissection of whole-body IS by its peripheral and liver components.

RW Access Increases the β-Oxidation Capacity Primarily in the Muscle of LFD-Fed Animals

The quantitative dissection of peripheral and liver IS allowed us to relate these to mitochondrial function in specific

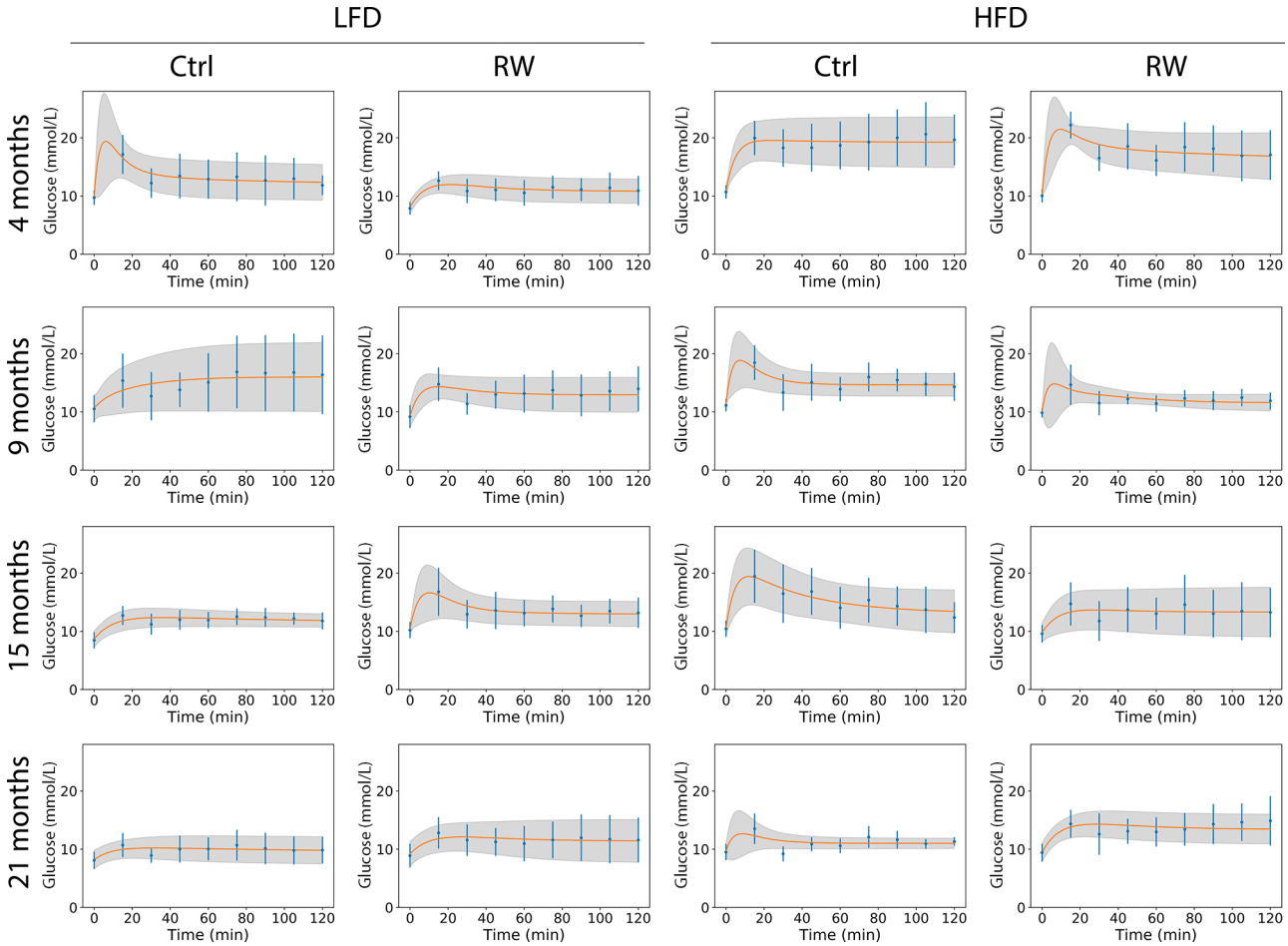

Figure 4—Curve fits of unlabeled glucose time courses during OGTT. Each column represents a different diet and activity group, whereas each row represents a different age. Mean ± SD for each time point are shown in blue. The average curve fit (C_2 in the model) is shown in orange, with the SD represented by the shaded area. n = 6–8 per group.

tissues. Alterations in mitochondrial fatty-acid β-oxidation can modulate lipid clearance and impact insulin resistance development (48,49). The content of CPT1B in the skeletal muscle declined with age ($P_{age} < 0.001$) in all analyzed groups (Fig. 7*A*), which aligns with results of an independent study (13). The HFD strongly upregulated muscle CPT1B content ($P_{diet} < 0.001$), whereas RW access increased it only in LFD animals ($P_{RW} < 0.01$ and $P_{RW \times diet} < 0.001$). In the skeletal muscle, the measured oxidative capacity with palmitoyl-CoA as substrate roughly correlated with the CPT1B levels (Fig. 7*C*, Supplementary Fig. 7A). However, LFD Ctrl mice did not show a decline in oxidative capacity with age, in contrast to the CPT1B level (compare with Fig. 7*A* and *C*). Of note, in the youngest and oldest groups, both CPT1B content and oxidative capacity followed the same pattern of age-dependent loss of flexibility to the HFD, as we previously noted (Supplementary Fig. 7*C* and *D*).

In the liver, CPT1A (liver isoform) content was also increased by the HFD ($P_{diet} < 0.05$), and declined with age (Fig. 7*B*), even though there was no effect of RW access. A correlation between CPT1A and oxidative capacity was also observed in the liver, albeit weaker than in the muscle (Fig. 7*D*, Supplementary Fig. 7*B*). In the liver, the oxidative capacity was decreased by age and enhanced by the HFD (for age and diet each, $P < 0.001$), with no clear RW access effect (Fig. 7*D*).

The steep decline of the IS-P between 4 and 9 months in the LFD groups (Fig. 6*C*) preceded the decline of CPT1B content of the muscle. Nevertheless, RW access increased CPT1B content and oxidative capacity predominantly in the 4-month-old LFD group, the same group in which it rescued the IS-P the most. The correlation between CPT1B content and IS-P in the LFD group had an R^2 of 0.55 (Supplementary Fig. 7*E*). which indicates that other factors contributed 45% to the modulation of peripheral IS by age and RW access. Altogether, the upregulation in β-oxidation capacity in the skeletal muscle by RW access only improved IS when there was no lipid overload (LFD groups).

DISCUSSION

Here, we dissected in detail how age, diet, physical activity, and their interaction affect peripheral and hepatic IS and how these are associated with the mitochondrial fatty-acid

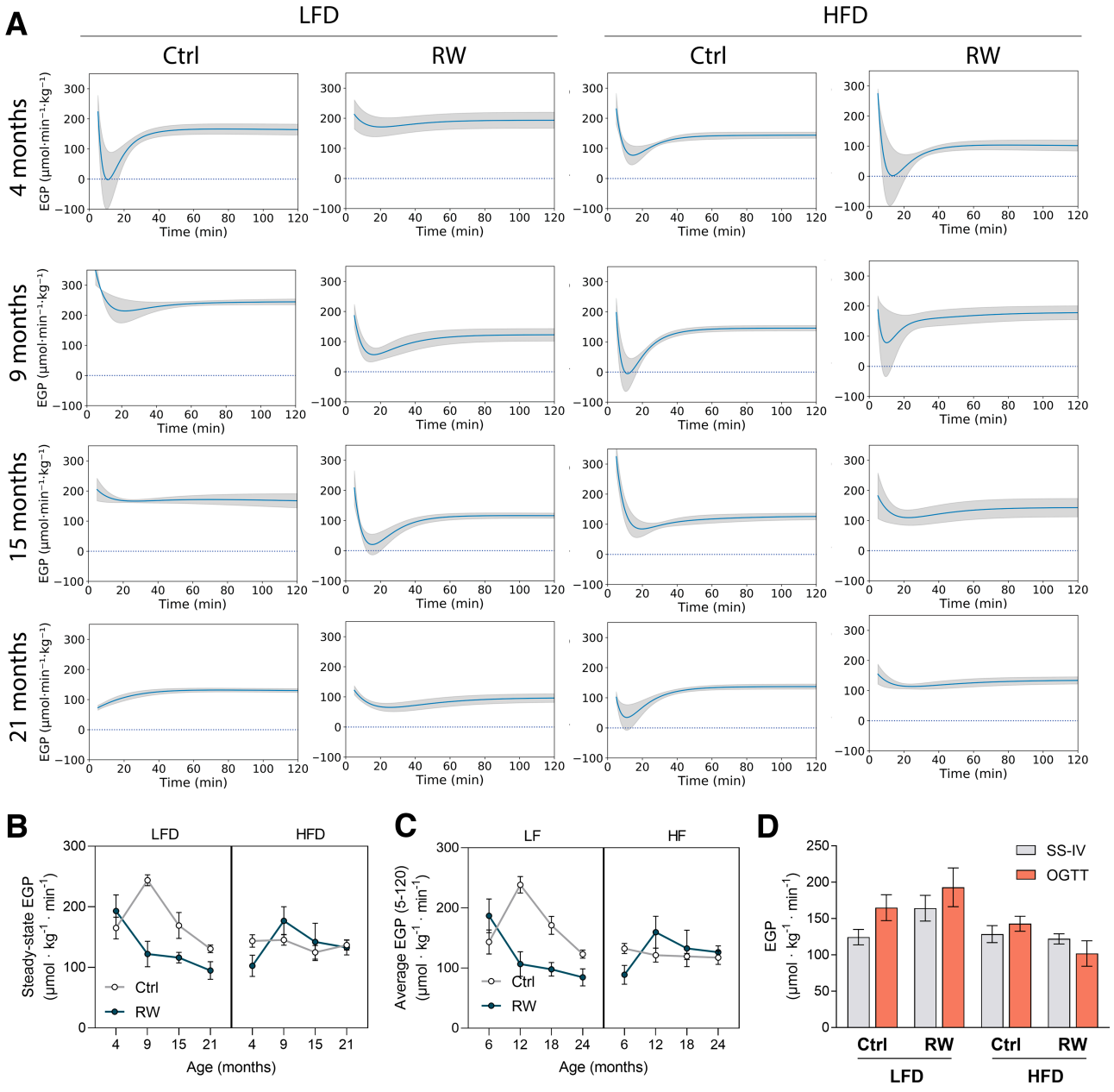

Figure 5—EGP is reduced by aging in the LFD group. Time courses for EGP (*A*). Each column represents a different diet and activity group, whereas each row represents a different age. Mean EGP (line) ± SEM (shaded area) data are shown per experimental group. Steady-state EGP values (*B*) calculated from the curves (mean ± SEM). Time-averaged EGP values (*C*) obtained from OGTT time frame (5–120 min; mean ± SEM). Comparison between steady-state EGP values (mean ± SD) obtained from the tracer OGTT in 4-month-old animals and SS-IV experiments conducted in the same animals at 6 months (*D*). *n* = 2–8 per group.

oxidation capacity. To our knowledge, such a comprehensive analysis has never been conducted before. The most surprising result was that physical activity rescued the hepatic IS in aging mice, with only a minor age-dependent effect on the muscle. In addition, these beneficial effects of RW access were only observable in the LFD group. In agreement with earlier results in the muscle (13), the HFD-dependent induction of CPT1 and mitochondrial fatty-acid oxidation were lost in aged mice, both in the muscle and in the liver. This loss of mitochondrial flexibility was not directly reflected in IS, suggesting that the latter also depends on other factors. Finally, RW access, which results in a chronic exercise regimen, rescued this age-dependent loss of CPT1B and oxidative capacity only in the skeletal muscle of LFD animals, the same diet group in which some improvement of peripheral IS was observed. An overview of the main findings is given in Table 1.

The computational model to analyze the tracer OGTT was inspired by the Oral Minimal Model for humans (37). A difference between mouse and human studies is that less frequent and smaller blood volumes can be obtained from mice (38). Recently, a more complex computational

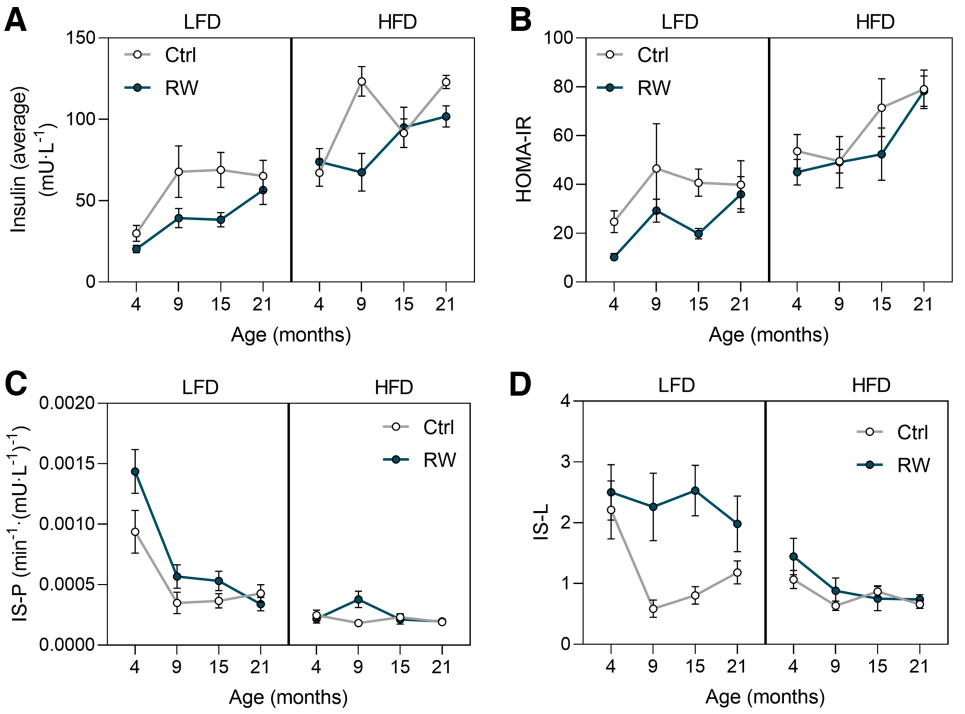

$$IS\text{-}P = \frac{k_2}{INS_{OGTT}} \qquad IS\text{-}L = \frac{\overline{EGP} \times \overline{INS_{OGTT}}}{EGP \times INS_{OGTT}}$$

Figure 6—Peripheral and central IS are regulated by age, diet, and RW access. Average insulin levels during the OGTT (0, 30, and 60 min) (*A*). HOMA-IR calculated from fasting glucose and fasting insulin levels (*B*). IS-P (*C*) and IS-L (*D*) for tracer OGTT, calculated according to the featured equations. INS_{OGTT} is the time-average insulin levels per animal; *EGP* is the time-average EGP per animal (5–120 min). $\overline{EGP}$ and $\overline{INS}_{OGTT}$ are the average of *EGP* and INS_{OGTT} values, respectively, for all 16 experimental groups. Data are shown as mean ± SEM; n = 2–8 per group.

model was fitted to mouse tracer-OGTT data that had been obtained with a similar experimental setup. The latter model included insulin-dependent and -independent glucose elimination (36). Although biologically more realistic, it is plausible that this higher complexity came at the expense of parameter identifiability (50), but this was not explicitly addressed (36). A limitation of the present study is that glucose bioavailability was considered constant, irrespective of age, diet, and physical exercise, even though this did not affect the relative differences between the groups. Moreover, the model does not accurately capture the initial dynamics of glucose absorption, given that transit compartments were not included. Despite these simplifications, the calculated steady-state fluxes were comparable to those obtained from independent steady-state infusion experiments. A final limitation concerns the use of only male mice because sex is known to play a role in the response to diet, age, and exercise (51,52).

Previously, peripheral IS has been defined as the ability of insulin to enhance glucose effectiveness (31). Because the latter is expressed by the apparent elimination rate constant k_2, we defined the peripheral IS as IS-P = k_2/INS_{OGTT}. This parameter has the same units as the previously described insulin action parameter (31). IS-P is reminiscent of the MISI (5,30). The MISI is defined as the slope of the glucose decay during the clearance phase of the OGTT divided by the average insulin concentration during the same period. The slope depends on glucose absorption and elimination, which, in turn, depend on the glucose concentration. In contrast to the glucose decay slope used to calculate the MISI, k_2 is specific for the elimination process and corrected for the glucose concentration. Similarly, the IS-L was adapted from an existing index for hepatic IS (29), the difference being that the IS-L analysis relies on the average response during the OGTT, whereas the classic analysis was based on fasting data. To capture the dynamics of hepatic and peripheral IS during the OGTT would require more data points and additional assumptions, or multiple tracer experiments (45).

HFDs have long been used to induce obesity and insulin resistance in animal models (53). In agreement with this, the HFD decreased both IS-P and IS-L (Fig. 6*C* and *D*). In previous studies, aging exacerbated HFD-induced insulin resistance (11,12). In this study, this was confirmed by the HOMA-IR, and it could be specifically attributed to the hepatic insulin response, as quantified by the IS-L. The peripheral insulin response (as indicated by the IS-P) was,

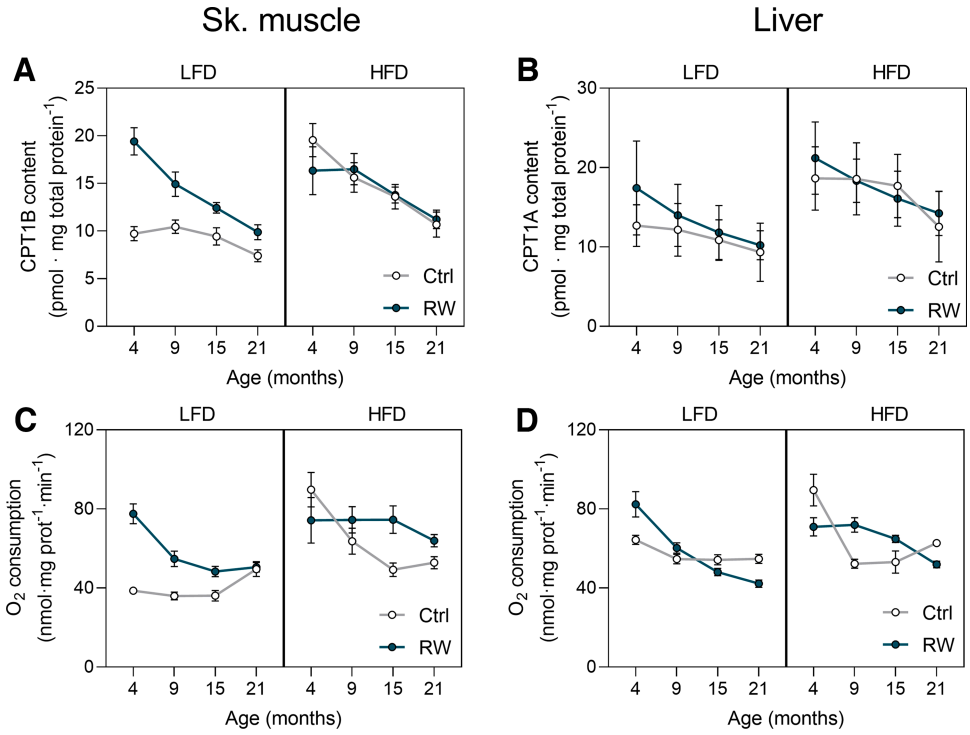

Figure 7—CPT1 content and oxidative capacity decline during aging. CPT1B protein content expressed per total skeletal (Sk.) muscle protein (*A*). CPT1A protein content expressed per total liver protein (*B*). Oxidative capacity (maximal ADP-stimulated O_2 consumption) with the use of palmitoyl-CoA, carnitine, and malate as substrates for skeletal muscle (*C*) and liver (*D*) expressed per total tissue protein. CPT1B protein content was available from Stolle et al. (26). Skeletal muscle oxidative capacity data were reproduced from the same study (26). Data are shown as mean ± SEM; n = 4–8 per group.

however, equally low in all HFD groups, in contrast to our earlier findings that HFD-induced peripheral insulin resistance was aggravated by age (13). The studies differ, however, in terms of *1*) diet duration, timing, and composition; and *2*) mouse strain.

Despite the just-mentioned differences in experimental setup, the CPT1B content and the mitochondrial capacity to oxidize fatty acids in the skeletal muscle recapitulate our previous findings (Supplementary Fig. 7*C* and *D*). In both studies, older mice showed less flexibility to upregulate the fatty-acid oxidation capacity in the muscle when fed an HFD (13). A similar pattern was observed in the liver (Fig. 7*D*). This mechanism was proposed to underlie the high muscle-lipid accumulation in older HFDanimals, consequently aggravating insulin resistance. In the present study, however, the IS-P decline with age preceded the drop in CPT1B content and fatty-acid oxidation capacity (Fig. 7*A* and *C*). Consequently, additional insulin resistance–inducing mechanisms likely underlie the observed phenotype.

In this study, RW access was present throughout the life of the mice and was not removed during the OGTT time frame. However, because the mice did not exercise during the day when the OGTT was conducted (Supplementary Fig. 1), we address here the effects of chronic, and not

Table 1—Overview of main findings and strength of associations*

Parameter	Age (old vs. young)	Diet (HFD vs. LFD)	Exercise (RW vs. Ctrl)
k_2 (clearance rate)	Diet-dependent effect	↓	—
EGP	↓↓	—	↓ (LFD group)
IS-P	↓↓ (LFD group)	↓↓↓	↑
IS-L	↓	↓↓	↑ (LFD group)
Oxidative capacity quadriceps	↓↓	↑↑↑	↑
Oxidative capacity liver	↓↓↓↓	↑	Age-dependent effect

*Arrows represent the direction of change (increase vs. decrease). The number of arrows represents to what extent a result is explained by each variable. 1 arrow: 0–10% variance, 2 arrows:10–20% variance, 3 arrows: 20–30% variance, 4 arrows: >30% variance, dash: no significant changes. Groups between parentheses indicate that the variance is further explained by interaction with the specified group.

acute, exercise on IS. The peripheral IS was barely enhanced by exercise in older groups, which corroborates the findings of Short et al. in humans (24). However, several human studies have pointed to resistance or high-intensity aerobic training as strategies to improve IS in the elderly (3,54,55). Moreover, training regimens that result in weight loss could be a more effective strategy (56). In the present cohort, weight was maintained (26). Different explanations might underlie the heterogeneity of outcomes. First, the type and duration of exercise differed among studies. Second, the quantification of insulin resistance ranged from simple whole-body HOMA-IR quantification to more complex tracer and clamp studies. Third, mice run less as they grow older (57,58), which was confirmed for the mice used here, especially for the HFD groups, and described in earlier reports about the same cohort (26,35). Nevertheless, voluntary running promoted beneficial health adaptations, including mitochondrial remodeling (25,26). We observed, however, that the insulin-desensitizing effects of the HFD outweighed the insulin-sensitizing response to endurance exercise. The net effect of diet and exercise on the insulin-signaling cascade dictates glucose uptake rates and, consequently, insulin resistance development or prevention.

Lifelong RW access decreased the EGP in the LFD group (Fig. 5*B* and *C*). This corroborates previous findings after a short-term RW intervention in mice (32). Moreover, the RW-access intervention remarkably sustained a prolonged, high hepatic IS during aging, albeit only in the LFD group. This was in stark contrast with the muscle, in which RW access did not prevent the age-dependent decline of the IS-P. The increase of the IS-L by RW access was not associated with CPT1A content or oxidative capacity. Rather, it may be attributed to the aforementioned increased capacity of hepatic glucose uptake, irrespective of insulin. Alternatively, it may derive from the action of insulin-sensitizing myokines, which can communicate the effect of exercise from the muscle to the liver (59).

In summary, based on a simple two-compartment model, EGP and muscle- and liver-specific IS could be reliably estimated from a noninvasive tracer-based OGTT. Hepatic and peripheral IS were both similarly decreased by aging and an HFD. In LFD-fed mice, exercise enhanced peripheral IS mostly in young animals and completely prevented the age-dependent loss of hepatic IS. These results, together with the applied methodology, may contribute to future research on the role of mitochondria in insulin resistance.

Acknowledgments. We thank Maaike Oosterveer and Angela Tol of the Laboratory of Pediatrics of the University Medical Center Groningen for valuable discussions.

Funding. This study was funded by a grant from the Netherlands Organization for Scientific Research (NWO; grant 853.00.110), by DSM Nutritional products in the framework of the Complexity program (grant 645.001.001/3501), a University Medical Center Groningen (UMCG) MD/PhD fellowship to C.J.V., and a UMCG–Graduate School of Medical Sciences PhD fellowship to M.A.V.-L.

Duality of Interest. No potential conflicts of interest relevant to this article were reported.

Author Contributions. M.A.V.-L., S.K., and B.M.B. developed the computational model, advised by A.C.R., J.C., F.A., A.T., and T.H.v.D. conducted animal experiments. M.A.V.-L., A.C.R., and S.K. conducted data analysis. T.H.v.D. analyzed steady-state labeling data. J.C.W. conducted proteomics experiments. C.J.V. and R.H.J.B. contributed with the experiments on bioavailability. A.K.G., D.-J.R., G.v.D., and B.M.B. conceptualized and supervised the project. M.A.V.-L. and B.M.B. wrote the manuscript. All authors read and approved the final manuscript. B.M.B. is the guarantor of this work and, as such, had full access to all the data in the study and take responsibility for the integrity of the data and the accuracy of the data analysis.

Prior Presentation. Parts of this study were presented orally at the Bioinformatics & Systems Biology Conference 2021, virtual, 15–16 June 2021; and at the International Study Group for Systems Biology 2022, Innsbruck, Austria, 19–23 September 2022.

References

1. Barzilai N, Huffman DM, Muzumdar RH, Bartke A. The critical role of metabolic pathways in aging. Diabetes 2012;61:1315–1322
2. Petersen MC, Shulman GI. Mechanisms of insulin action and insulin resistance. Physiol Rev 2018;98:2133–2223
3. Jiahao L, Jiajin L, Yifan L. Effects of resistance training on insulin sensitivity in the elderly: a meta-analysis of randomized controlled trials. J Exerc Sci Fit 2021;19:241–251
4. DeFronzo RA, Tripathy D. Skeletal muscle insulin resistance is the primary defect in type 2 diabetes. Diabetes Care 2009;32(Suppl. 2):S157–S163
5. Abdul-Ghani MA, Matsuda M, Balas B, DeFronzo RA. Muscle and liver insulin resistance indexes derived from the oral glucose tolerance test. Diabetes Care 2007;30:89–94
6. Kowalski GM, Bruce CR. The regulation of glucose metabolism: implications and considerations for the assessment of glucose homeostasis in rodents. Am J Physiol Endocrinol Metab 2014;307:E859–E871
7. Surwit RS, Feinglos MN, Rodin J, et al. Differential effects of fat and sucrose on the development of obesity and diabetes in C57BL/6J and A/J mice. Metabolism 1995;44:645–651
8. Samuel VT, Shulman GI. The pathogenesis of insulin resistance: integrating signaling pathways and substrate flux. J Clin Invest 2016;126:12–22
9. Goodpaster BH. Mitochondrial deficiency is associated with insulin resistance. Diabetes 2013;62:1032–1035
10. Muoio DM. Metabolic inflexibility: when mitochondrial indecision leads to metabolic gridlock. Cell 2014;159:1253–1262
11. Koonen DP, Sung MM, Kao CK, et al. Alterations in skeletal muscle fatty acid handling predisposes middle-aged mice to diet-induced insulin resistance. Diabetes 2010;59:1366–1375
12. Nunes-Souza V, César-Gomes CJ, Da Fonseca LJ, Guedes GdaS, Smaniotto S, Rabelo LA. Aging increases susceptibility to high fat diet-induced metabolic syndrome in C57BL/6 mice: improvement in glycemic and lipid profile after antioxidant therapy. Oxid Med Cell Longev 2016;2016:1987960
13. Vieira-Lara MA, Dommerholt MB, Zhang W, et al. Age-related susceptibility to insulin resistance arises from a combination of CPT1B decline and lipid overload. BMC Biol 2021;19:154
14. Gong Z, Tas E, Yakar S, Muzumdar R. Hepatic lipid metabolism and non-alcoholic fatty liver disease in aging. Mol Cell Endocrinol 2017;455:115–130
15. Eaton S. Control of mitochondrial β-oxidation flux. Prog Lipid Res 2002;41:197–239
16. Larsson L, Degens H, Li M, et al. Sarcopenia: aging-related loss of muscle mass and function. Physiol Rev 2019;99:427–511
17. Cleasby ME, Jamieson PM, Atherton PJ. Insulin resistance and sarcopenia: mechanistic links between common co-morbidities. J Endocrinol 2016;229:R67–R81

18. Mann S, Beedie C, Balducci S, et al. Changes in insulin sensitivity in response to different modalities of exercise: a review of the evidence. Diabetes Metab Res Rev 2014;30:257–268
19. Bacchi E, Negri C, Zanolin ME, et al. Metabolic effects of aerobic training and resistance training in type 2 diabetic subjects: a randomized controlled trial (the RAED2 study). Diabetes Care 2012;35:676–682
20. Snijders T, Verdijk LB, van Loon LJC. The impact of sarcopenia and exercise training on skeletal muscle satellite cells. Ageing Res Rev 2009;8: 328–338
21. Egan B, Zierath JR. Exercise metabolism and the molecular regulation of skeletal muscle adaptation. Cell Metab 2013;17:162–184
22. Joseph AM, Adhihetty PJ, Leeuwenburgh C. Beneficial effects of exercise on age-related mitochondrial dysfunction and oxidative stress in skeletal muscle. J Physiol 2016;594:5105–5123
23. Phielix E, Meex R, Ouwens DM, et al. High oxidative capacity due to chronic exercise training attenuates lipid-induced insulin resistance. Diabetes 2012;61:2472–2478
24. Short KR, Vittone JL, Bigelow ML, et al. Impact of aerobic exercise training on age-related changes in insulin sensitivity and muscle oxidative capacity. Diabetes 2003;52:1888–1896
25. Manzanares G, Brito-da-Silva G, Gandra PG. Voluntary wheel running: patterns and physiological effects in mice. Braz J Med Biol Res 2018; 52:e7830
26. Stolle S, Ciapaite J, Reijne AC, et al. Running-wheel activity delays mitochondrial respiratory flux decline in aging mouse muscle via a post-transcriptional mechanism. Aging Cell 2018;17:1–11
27. Trefts E, Williams AS, Wasserman DH. Exercise and the regulation of hepatic metabolism. Prog Mol Biol Transl Sci 2015;135:203–225
28. Gregory JM, Muldowney JA, Engelhardt BG, et al. Aerobic exercise training improves hepatic and muscle insulin sensitivity, but reduces splanchnic glucose uptake in obese humans with type 2 diabetes. Nutr Diabetes 2019;9:25
29. Matsuda M, DeFronzo RA. Insulin sensitivity indices obtained from oral glucose tolerance testing: comparison with the euglycemic insulin clamp. Diabetes Care 1999;22:1462–1470
30. O'Donovan SD, Lenz M, Goossens GH, et al. Improved quantification of muscle insulin sensitivity using oral glucose tolerance test data: the MISI Calculator. Sci Rep 2019;9:9388
31. Vicini P, Caumo A, Cobelli C. The hot IVGTT two-compartment minimal model: indexes of glucose effectiveness and insulin sensitivity. Am J Physiol 1997;273:E1024–E1032
32. Allerton TD, Kowalski G, Hang H, Stephens J. Dynamic glucose disposal is driven by reduced endogenous glucose production in response to voluntary wheel running: a stable isotope approach. Am J Physiol Endocrinol Metab 2020;319:E2–E10
33. Dalla Man C, Caumo A, Basu R, Rizza R, Toffolo G, Cobelli C. Minimal model estimation of glucose absorption and insulin sensitivity from oral test: validation with a tracer method. Am J Physiol Endocrinol Metab 2004;287:E637–E643
34. Thomaseth K, Pavan A, Berria R, Glass L, DeFronzo R, Gastaldelli A. Model-based assessment of insulin sensitivity of glucose disposal and endogenous glucose production from double-tracer oral glucose tolerance test. Comput Methods Programs Biomed 2008;89:132–140
35. Reijne AC, Talarovicova A, Ciapaite J, et al. Running wheel access fails to resolve impaired sustainable health in mice feeding a high fat sucrose diet. Aging (Albany NY) 2019;11:1564–1579
36. Dommerholt MB, Blankestijn M, Vieira-Lara MA, et al. Short-term protein restriction at advanced age stimulates FGF21 signalling, energy expenditure and browning of white adipose tissue. FEBS J 2021;288:2257–2277
37. Cobelli C, Dalla Man C, Toffolo G, Basu R, Vella A, Rizza R. The oral minimal model method. Diabetes 2014;63:1203–1213
38. van Dijk TH, Boer TS, Havinga R, Stellaard F, Kuipers F, Reijngoud D-J. Quantification of hepatic carbohydrate metabolism in conscious mice using serial blood and urine spots. Anal Biochem 2003;322:1–13
39. Mildaziene V, Nauciene Z, Baniene R, Grigiene J. Multiple effects of 2,2′,5,5′-tetrachlorobiphenyl on oxidative phosphorylation in rat liver mitochondria. Toxicol Sci 2002;65:220–227
40. Wolters JC, Ciapaite J, van Eunen K, et al. Translational targeted proteomics profiling of mitochondrial energy metabolic pathways in mouse and human samples. J Proteome Res 2016;15:3204–3213
41. Gnaiger E, Kuznetsov V, Schneeberger S, et al. Mitochondria in the cold. In Life in the Cold. Heldmaier G, Klingenspor M, Eds., York, UK, Springer Nature, 2000, pp. 431–442
42. Ferrannini E, Wahren J, Felig P, DeFronzo RA. The role of fractional glucose extraction in the regulation of splanchnic glucose metabolism in normal and diabetic man. Metabolism 1980;29:28–35
43. Abumrad NN, Cherrington AD, Williams PE, Lacy WW, Rabin D. Absorption and disposition of a glucose load in the conscious dog. Am J Physiol 1982; 242:E398–E406
44. Balcombe JP, Barnard ND, Sandusky C. Laboratory routines cause animal stress. Contemp Top Lab Anim Sci 2004;43:42–51
45. Man CD, Toffolo G, Basu R, Rizza RA, Cobelli C. Use of labeled oral minimal model to measure hepatic insulin sensitivity. Am J Physiol Endocrinol Metab 2008;295:E1152–E1159
46. Muniyappa R, Lee S, Chen H, Quon MJ. Current approaches for assessing insulin sensitivity and resistance in vivo: advantages, limitations, and appropriate usage. Am J Physiol Endocrinol Metab 2008;294:E15–E26
47. Lewis GF, Carpentier AC, Pereira S, Hahn M, Giacca A. Direct and indirect control of hepatic glucose production by insulin. Cell Metab 2021;33:709–720
48. Bruce CR, Hoy AJ, Turner N, et al. Overexpression of carnitine palmitoyltransferase-1 in skeletal muscle is sufficient to enhance fatty acid oxidation and improve high-fat diet-induced insulin resistance. Diabetes 2009; 58:550–558
49. Keung W, Ussher JR, Jaswal JS, et al. Inhibition of carnitine palmitoyltransferase-1 activity alleviates insulin resistance in diet-induced obese mice. Diabetes 2013;62:711–720
50. Rizza RA, Toffolo G, Cobelli C. Accurate measurement of postprandial glucose turnover: why is it difficult and how can it be done (relatively) simply? Diabetes 2016;65:1133–1145
51. Holcomb LE, Rowe P, O'Neill CC, DeWitt EA, Kolwicz SC Jr. Sex differences in endurance exercise capacity and skeletal muscle lipid metabolism in mice. Physiol Rep 2022;10:e15174
52. Kane AE, Sinclair DA, Mitchell JR, Mitchell SJ. Sex differences in the response to dietary restriction in rodents. Curr Opin Physiol 2018;6:28–34
53. Kleinert M, Clemmensen C, Hofmann SM, et al. Animal models of obesity and diabetes mellitus. Nat Rev Endocrinol 2018;14:140–162
54. DiPietro L, Dziura J, Yeckel CW, Neufer PD. Exercise and improved insulin sensitivity in older women: evidence of the enduring benefits of higher intensity training. J Appl Physiol (1985) 2006;100:142–149
55. Kitamura I, Takeshima N, Tokudome M, Yamanouchi K, Oshida Y, Sato Y. Effects of aerobic and resistance exercise training on insulin action in the elderly. Geriatr Gerontol Int 2003;3:50–55
56. Coker RH, Hays NP, Williams RH, et al. Exercise-induced changes in insulin action and glycogen metabolism in elderly adults. Med Sci Sports Exerc 2006;38:433–438
57. White Z, Terrill J, White RB, et al. Voluntary resistance wheel exercise from mid-life prevents sarcopenia and increases markers of mitochondrial function and autophagy in muscles of old male and female C57BL/6J mice. Skelet Muscle 2016;6:45
58. Figueiredo PA, Powers SK, Ferreira RM, Amado F, Appell HJ, Duarte JA. Impact of lifelong sedentary behavior on mitochondrial function of mice skeletal muscle. J Gerontol A Biol Sci Med Sci 2009;64:927–939
59. Raschke S, Eckel J. Adipo-myokines: two sides of the same coin–mediators of inflammation and mediators of exercise. Mediators Inflamm 2013;2013:320724